Posterior Fossa Malformations

Mariasavina Severino, MD[a,*], Thierry A.G.M. Huisman, MD[b]

KEYWORDS

• Brain stem • Cerebellum • Midbrain-hindbrain • Malformations • Neuroimaging • MR imaging • DTI • Children

KEY POINTS

- Progress in neuroimaging and genetics in the last decades has led to a significant improvement/refinement in the definition/classification of cerebellar and brainstem malformations.
- Neuroimaging plays a key role in the diagnostic workup of children with cerebellar and brainstem malformations.
- Advanced neuroimaging techniques, such as diffusion tensor imaging, have greatly improved the characterization of posterior fossa malformations, demonstrating white matter tract anomalies due to disrupted or altered axonal path-finding.

INTRODUCTION

Posterior fossa malformations include a wide spectrum of heterogeneous conditions caused by disruption of molecular pathways involved in cerebellar and brainstem formation, secondary to gene mutations, teratogens, or combined effects.[1–3] In the last few decades, progress in neuroimaging techniques, neurogenetic analysis, and mouse model research has led to a significant improvement in the definition and classification of these malformations as well as in the recognition of novel disorders. Several classification schemes have been proposed based on neuroimaging, molecular/genetic criteria, and developmental biological criteria.[1–3] However, posterior fossa malformations remain a challenging diagnosis, because they are uncommon and less well known compared with supratentorial anomalies. Moreover, children present with a wide spectrum of neurologic and systemic manifestations, resulting in a highly variable clinical phenotype.[1,2] Therefore, knowledge of neuroimaging features is fundamental for recognizing these malformations correctly.[1–5]

Here, the authors discuss imaging techniques and protocols, describe the normal anatomy of the posterior fossa and its contents, and review the characteristic neuroimaging features of posterior fossa malformations, based on a simplified classification: (a) Predominantly cerebellar malformations, (b) Combined cerebellar and brainstem malformations, and (c) Predominantly brainstem malformations.[2]

IMAGING TECHNIQUES AND NORMAL ANATOMY

MR imaging is the imaging modality of choice allowing detailed evaluation of the anatomy of the posterior fossa and its contents (**Fig. 1**A–C, **Table 1**).[1–3] Computed tomography has a limited role and is mainly used for the detection of bony anomalies and/or calcifications that may remain undetected on MR imaging. In the last decade, advanced MR imaging techniques, such as diffusion tensor imaging (DTI) and fiber tractography (FT), allowed in vivo demonstration of normal brainstem and cerebellar microstructural anatomy (**Fig. 1**D–G). DTI and FT proved to be especially

Disclosure: The authors have nothing to disclose.
[a] Neuroradiology Unit, IRCCS Istituto Giannina Gaslini, via Gaslini 5, Genoa 16147, Italy; [b] Edward B. Singleton Department of Radiology, Texas Children's Hospital, 6701 Fannin Street, Suite 470, Houston, TX 77030, USA
* Corresponding author.
E-mail address: MariasavinaSeverino@gaslini.org

Neuroimag Clin N Am 29 (2019) 367–383
https://doi.org/10.1016/j.nic.2019.03.008

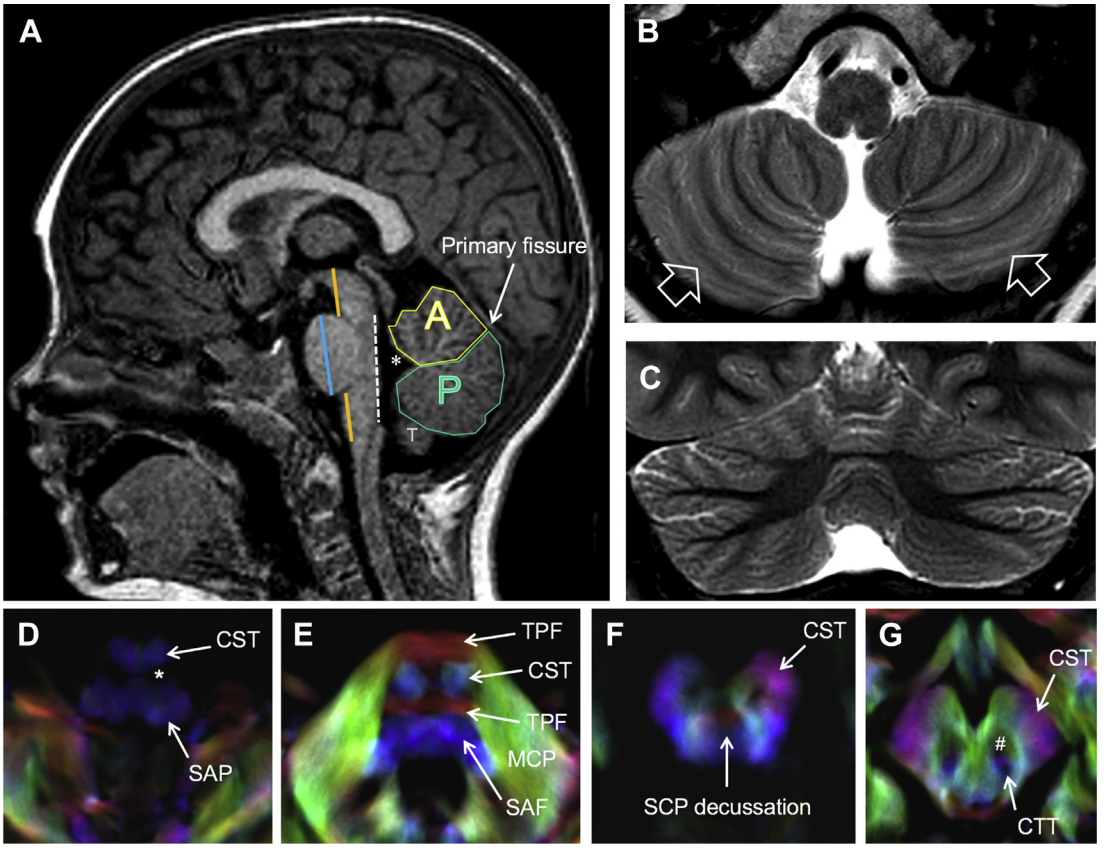

Fig. 1. Normal posterior fossa anatomy. (*A*) On midline sagittal T1-weighted MR imaging, the rostrocaudal length of the ventral pons (*blue line*) is approximately 1.5 that of the midbrain, whereas the rostrocaudal length of the midbrain should be roughly the same as that of the medulla (*orange lines*). The posterior margin of the brainstem extending from the caudal sylvian aqueduct to the obex should be a straight line (*dotted line*). The fastigium should lie just below the midpoint of the ventral pons (*asterisks*). The vermis is divided into anterior (A) and posterior (P) parts by the primary fissure. (*B*) Axial and (*C*) coronal T2-weighted MR images show the normal size and morphology of the cerebellar hemispheres. The cerebellar folia run parallel to the calvarium (onionlike configuration; *arrows*). Coronal images show fissures radiating toward the cerebellar nuclei. (*D–G*) Axial directionally encoded color fractional anisotropy (FA) maps, magnified view at 4 brainstem levels (rostral medulla, middle pons, middle midbrain, and rostral midbrain). Conventional color scheme: blue (inferior-superior), green (anteroposterior), and red (left-right). CCT, central tegmental tract; CST, corticospinal tract; MCP, middle cerebellar peduncles; SAF, somatosensory ascending fibers; TPF, transverse pontocerebellar fibers. *, Inferior olivary nucleus; #, red nucleus.

helpful to study white matter anomalies secondary to axonal path-finding disorders.[4–7] Finally, congenital abnormalities of the cerebellum and brainstem are progressively diagnosed by prenatal ultrasound and MR imaging. Fetal MR imaging generally includes single-shot T2-weighted, T1-weighted, and diffusion-weighted sequences.[8]

Predominantly Cerebellar Malformations

Dandy-Walker malformation

Dandy-Walker malformation (DWM) is defined by a cystic enlargement of the fourth ventricle associated with hypoplasia/agenesis of the vermis. It occurs sporadically in 1:25,000 to 35,000 live births.[9–11] Patients present in the first months of life with symptoms of intracranial hypertension and macrocephaly. DWM may be isolated or may be part of numerous chromosomal anomalies or Mendelian disorders. Interestingly, FOXC1 mutations resulting in dysgenesis of both the cerebellum and its overlying mesenchyme may cause DWM.[9]

On imaging, DWM is characterized by the following[10,11]:

- Upward and counterclockwise rotation of a hypoplastic/agenetic superior vermis
- Cystic dilatation of the fourth ventricle

Table 1
Recommended diagnostic MR imaging protocol

Sequence	Plane	Key Role
Isotropic 3D T1-WI	Multiplanar reformation	High-resolution anatomic information
2 or 3 mm 2D T2-WI	Axial, coronal	Detailed evaluation of cerebellar foliation, cortex, gray-white matter differentiation, dentate and cranial nerve nuclei
2D or 3D FLAIR images	Axial, coronal	Depiction of signal abnormalities
3D heavily T2-WI (CISS, DRIVE, FIESTA)	Multiplanar reformation	Evaluation of cranial nerves, inner ear, ventricular outlets
Susceptibility-weighted imaging	Axial	Highly sensitive for blood products and calcifications
DTI FT	Multiplanar reformation	Qualitative and quantitative information about white matter microstructure and architecture

Abbreviations: CISS, constructive interference in steady state; DRIVE, driven equilibrium; FIESTA, Fast Imaging Employing Steady-state Acquisition; FLAIR, Fluid Attenuated Inversion Recovery; WI, weighted images.

- Enlarged posterior fossa with varying degrees of upward displacement of transverse sinuses, tentorium, and torcular Herophili ("torcular-lambdoid inversion")
- Variable hypoplasia and anterolateral displacement of the cerebellar hemispheres
- Supratentorial hydrocephalus (about 90% of cases)
- Additional brain malformations, including callosal dysgenesis or agenesis, occipital encephalocele, polymicrogyria, and gray matter heterotopias (30%–50% of patients).

The first 3 findings are consistently present and required for diagnosis (Fig. 2).

In addition, various anomalies may coexist outside of the central nervous system (CNS), including polydactyly and cardiac anomalies.

Differential diagnoses of DWM include the following (Fig. 3, Table 2):

- Blake pouch cyst
- Mega cisterna magna
- Posterior fossa arachnoid cyst
- Isolated vermian hypoplasia

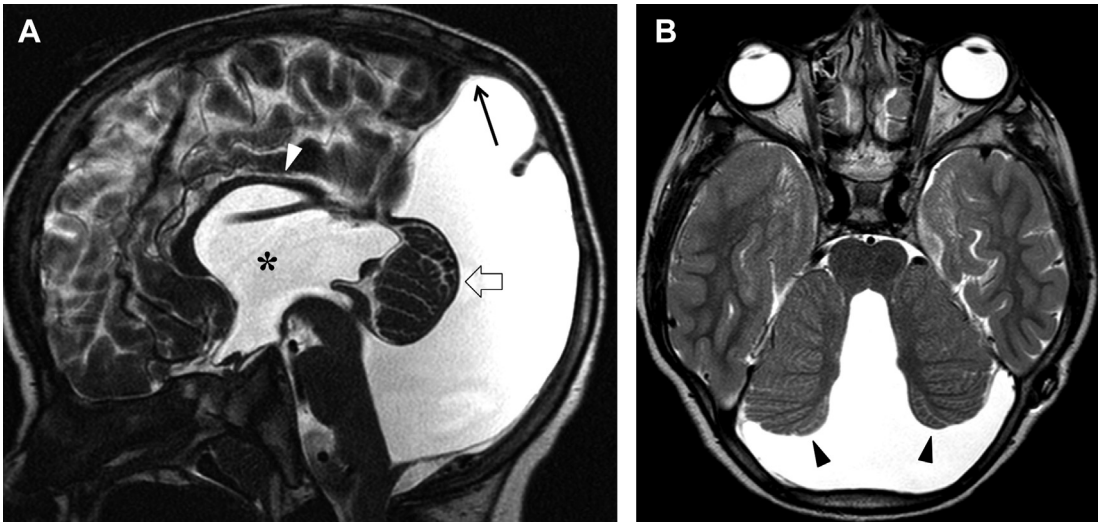

Fig. 2. DWM. (*A*) Sagittal and (*B*) axial T2-weighted MR images show upward and counterclockwise rotation of a hypoplastic vermis (*open arrow*), cystic dilatation of the fourth ventricle, lateral displacement of cerebellar hemispheres (*black arrowheads*), and torcular-lamboid inversion (*arrow*). Note the supratentorial hydrocephalus (*asterisk*), callosal hypoplasia (*white arrowhead*), and hypertelorism.

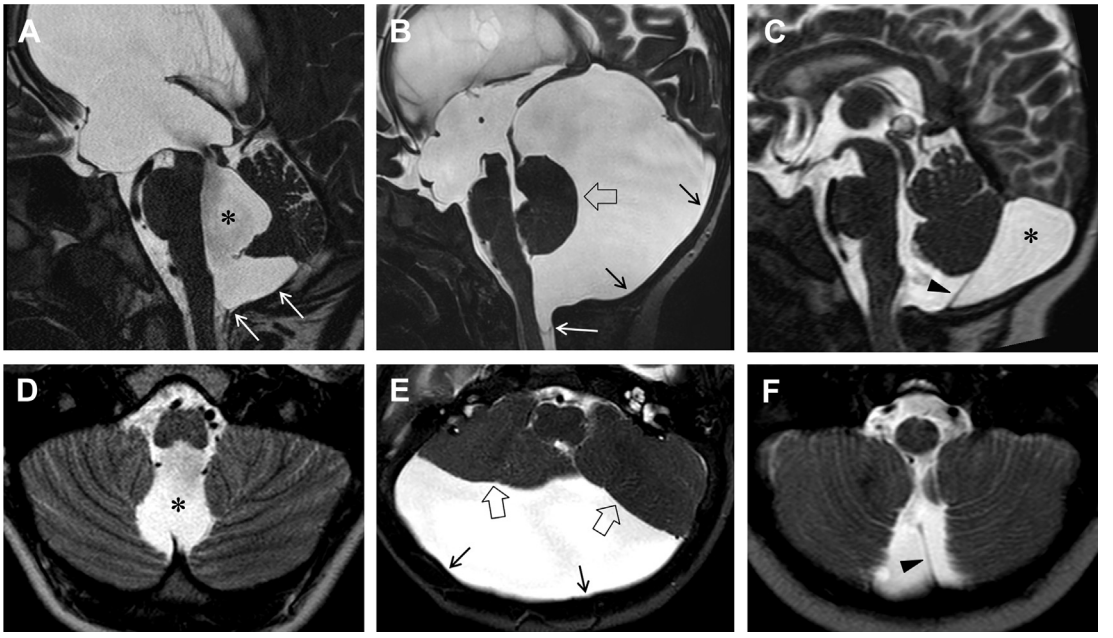

Fig. 3. Posterior fossa cystic malformations. (*A*) Midsagittal and (*D*) axial T2-weighted MR images of a child with a Blake pouch cyst reveal enlargement of the fourth ventricle (*asterisks*), which communicates with an infravermian cystic compartment corresponding to the Blake pouch cyst (*arrows*), a normal vermis, and tetraventricular hydrocephalus. (*B*) Midsagittal and (*E*) axial T2-weighted MR images of a child with a retrovermian arachnoid cyst demonstrate a CSF isointense cyst with posterior fossa enlargement, occipital bone scalloping (*black arrows*), mass effect on normal-appearing vermis and hemispheres (*open arrows*), normal fourth ventricle, and supratentorial hydrocephalus. Note the inferior cystic wall herniating through the foramen magnum (*white arrow*). (*C*) Midsagittal and (*F*) axial T2-weighted MR images of a child with megacisterna magna (*asterisk*) show normal vermis, fourth ventricle, and posterior fossa, remnants of the falx cerebelli (*arrowhead*), and absence of hydrocephalus.

Table 2
Differential diagnosis of cystic posterior fossa malformations

Malformation	Vermis	Fourth Ventricle	Posterior Fossa	Hydrocephalus	Occipital Scalloping
DWM	Hypoplastic, markedly rotated	Enlarged	Enlarged	Frequent	Yes
BPC	Normal, slightly upward rotated	Enlarged	Normal	Frequent	No
MCM	Normal, not rotated	Normal	Normal or slightly enlarged	Absent	Possible
PFAC	Normal (occasionally compressed), not rotated	Normal or reduced	Normal or slightly enlarged	Rare	Yes
IVH	Hypoplastic (inferior portion), occasionally slightly rotated	Normal or slightly enlarged	Normal	Absent	No

Abbreviations: BPC, blake pouch cyst; IVH, isolated vermian hypoplasia; MCM, mega cisterna magna; PFAC, posterior fossa arachnoid cyst.

Rhombencephalosynapsis

Rhombencephalosynapsis is defined by complete or partial absence of the vermis with fusion of the cerebellar hemispheres, dentate nuclei, and cerebellar peduncles.[12] The genetic basis of this malformation is unknown. However, a dorsoventral patterning defect in the rostral midline regions of rhombomere 1 is suspected.[2,3] Affected children present with signs of cerebellar dysfunction, including ataxia, abnormal eye movements, head stereotypies, and delayed motor development. Rhombencephalosynapsis is sporadic, and most of the patients are nonsyndromic. However, it may also occur in the setting of Gomez-Lopez-Hernandez syndrome (parietal alopecia, trigeminal anesthesia, and craniofacial dysmorphic signs) or VACTERL (Vertebral anomalies, Anal atresia, Cardiac defects, Tracheoesophageal fistula and/or Esophageal atresia, Renal anomalies, and Limb defects) association.[1–4,13]

The key neuroimaging findings are as follows (**Fig. 4**)[12–14]:

- Complete or partial absence of the vermis
- Fusion of the cerebellar hemispheres across the midline with cerebellar folia extending horizontally across the midline
- Fused superior cerebellar peduncles (SCP) and dentate nuclei
- Keyhole-shaped fourth ventricle
- Absence of the vermian primary fissure on midsagittal MR images

Of note, a variable degree of vermian formation and cerebellar hemisphere separation may be present (partial forms).

Supratentorial anomalies include the following[12–14]:

- Midline fusion of the colliculi (mesencephalosynapsis)
- Fused thalami (diencephalosynapsis)
- Hydrocephalus due to aqueductal stenosis/cerebrospinal fluid circulation disorder
- Corpus callosum dysgenesis
- Septum pellucidum agenesis
- Holoprosencephaly (rare)

Cerebellar hypoplasia and dysplasia

A malformed cerebellum may be hypoplastic (reduced cerebellar volume), dysplastic (abnormal cerebellar foliation, fissuration, and white matter architecture), or hypodysplastic (combined hypoplasia and dysplasia).[5] Each part of the cerebellum may be affected, resulting in global or partial cerebellar involvement. The clinical presentation is highly variable and mostly depends on the underlying disease.

On imaging, cerebellar dysplasia is characterized by variable combinations of the following (**Fig. 5**):

- Abnormal cerebellar foliation/fissuration, including defective, large, or vertical fissures (clefts), abnormal white matter arborization, and blurred gray-white matter interface
- Gray matter heterotopia within the cerebellar white matter
- Cortical thickening, resulting in an irregularly smooth, bumpy cerebellar surface
- Cortical-subcortical cysts usually isointense with cerebrospinal fluid (CSF) in all MR imaging sequences, varying in size, shape, and distribution[15]

Multiple genetic or acquired mechanisms are linked to cerebellar dysplasia, causing disruption of precursor cell division, neuronal migration, cortical layering, and fissure formation. Cerebellar dysplasia is therefore a nonspecific feature associated with several different conditions, such as Poretti-Boltshauser and

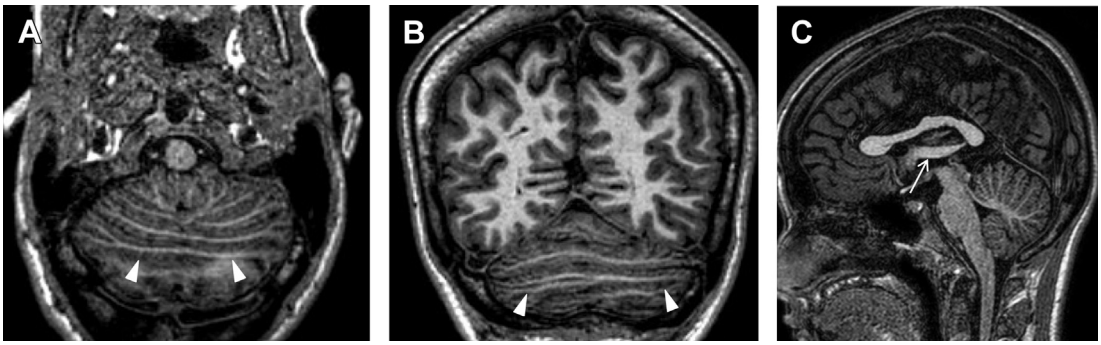

Fig. 4. Rhombencephalosynapsis. (*A*) Axial and (*B*) coronal-reformatted 3-dimensional (3D) T1-weighted MR images demonstrate absence of the vermis and fusion of the cerebellar hemispheres with characteristic uninterrupted horizontal extension of the cerebellar fissures and white matter across the midline (*arrowheads*). (*C*) Sagittal-reformatted 3D T1-weighted MR image reveals lack of definition of the normal vermian lobules resulting in a "cerebellar–not vermian–configuration." Note the low-lying fused fornices (*arrow*).

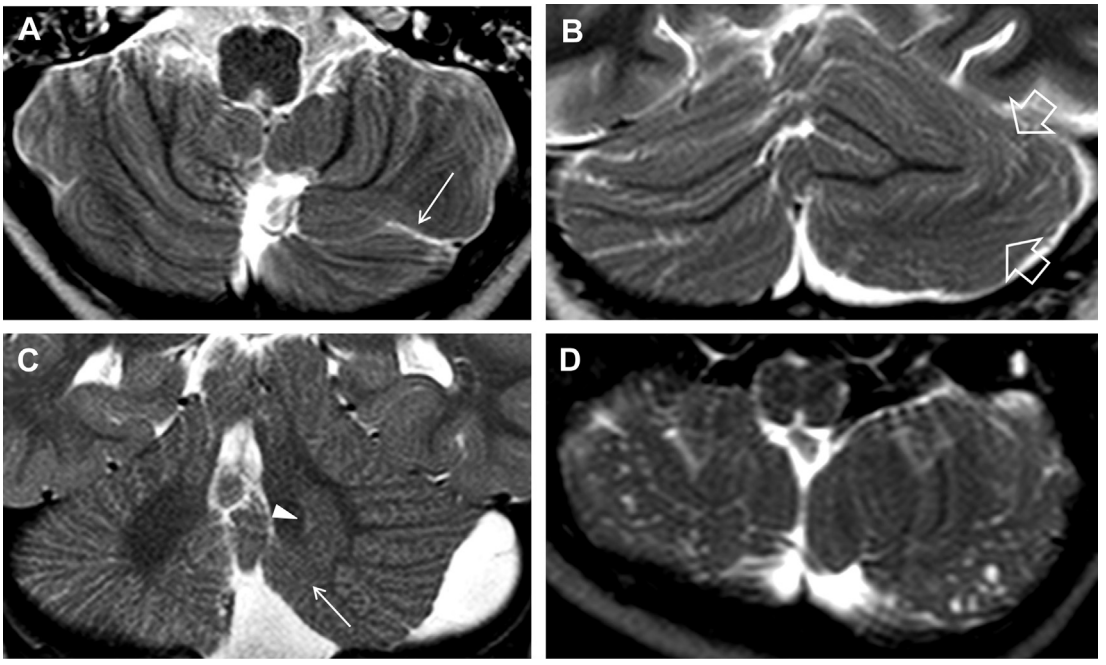

Fig. 5. Cerebellar dysplasia. (*A*) Axial and (*B*) coronal T2-weighted MR images reveal a lateral cleft (*arrow*) and abnormal cerebellar foliation and fissuration with loss of the normal white matter architecture (*open arrows*) in the left cerebellar hemispheres. (*C*) Coronal T2-weighted image reveals blurred gray-white matter interface (*arrow*) with gray matter heterotopia within the cerebellar white matter (*arrowhead*). (*D*) Axial T2-weighted MR image demonstrates bilateral abnormal foliation associated with multiple cortical-subcortical cysts.

Chudley-McCullogh syndromes (**Figs. 6** and **7**, **Table 3**).[16–20] Additional supratentorial findings are usually helpful to differentiate between the causative diseases (**Fig. 8**). However, in most cases, the exact pathogenesis remains unknown. Of note, unilateral cerebellar hypodysplasia is frequently the result of disruptive events, including prenatal/perinatal cerebellar hemorrhagic or ischemic infarcts, such as in preterm newborns or PHACE syndrome.[21]

Cerebellar and Brainstem Malformations

Pontocerebellar hypoplasia

The term "pontocerebellar hypoplasia" (PCH) is often used in a descriptive manner to refer to a reduction in volume of both cerebellum and pons. However, as conceptualized by Peter Barth, this term has been adopted to indicate a heterogeneous group of prenatal-onset neurodegenerative disorders, mainly but not exclusively affecting the cerebellum and pons.[22] To date, 11 subtypes of PCH with different phenotypes and pathogeneses have been identified (**Table 4**).[22,23] Of note, types 3, 8, and 11 have a nonprogressive course.

Characteristic MR imaging findings are listed as follows (**Fig. 9**):

- Cerebellar hypoplasia with superimposed atrophy
- Absence or significant reduction of the pontine prominence
- Normal or slightly reduced posterior fossa size
- Variable cerebral involvement, including atrophy and delayed myelination

The morphologic pattern of "pontocerebellar hypoplasia" is not specific to PCH: it has been shown in several malformations, disruptions (eg, in extreme prematurity), and neurometabolic diseases (eg, in congenital disorder of glycosylation type 1A).[21–28] In particular, severe cerebellar hypoplasia with pontine hypoplasia is frequently described in patients with mutations in the CASK, RELN, and VLDLR genes.

CASK encodes a multidomain scaffolding protein that regulates expression of genes involved in cortical development, such as RELN.[24] CASK mutations are inherited with an X-linked pattern, occur de novo, and more commonly affect female children, presumably because it is lethal in male children. Affected children present with ataxia, nystagmus, postnatal microcephaly, severe cognitive impairment, seizures, retinopathy, sensorineural hearing loss, and (inconsistently)

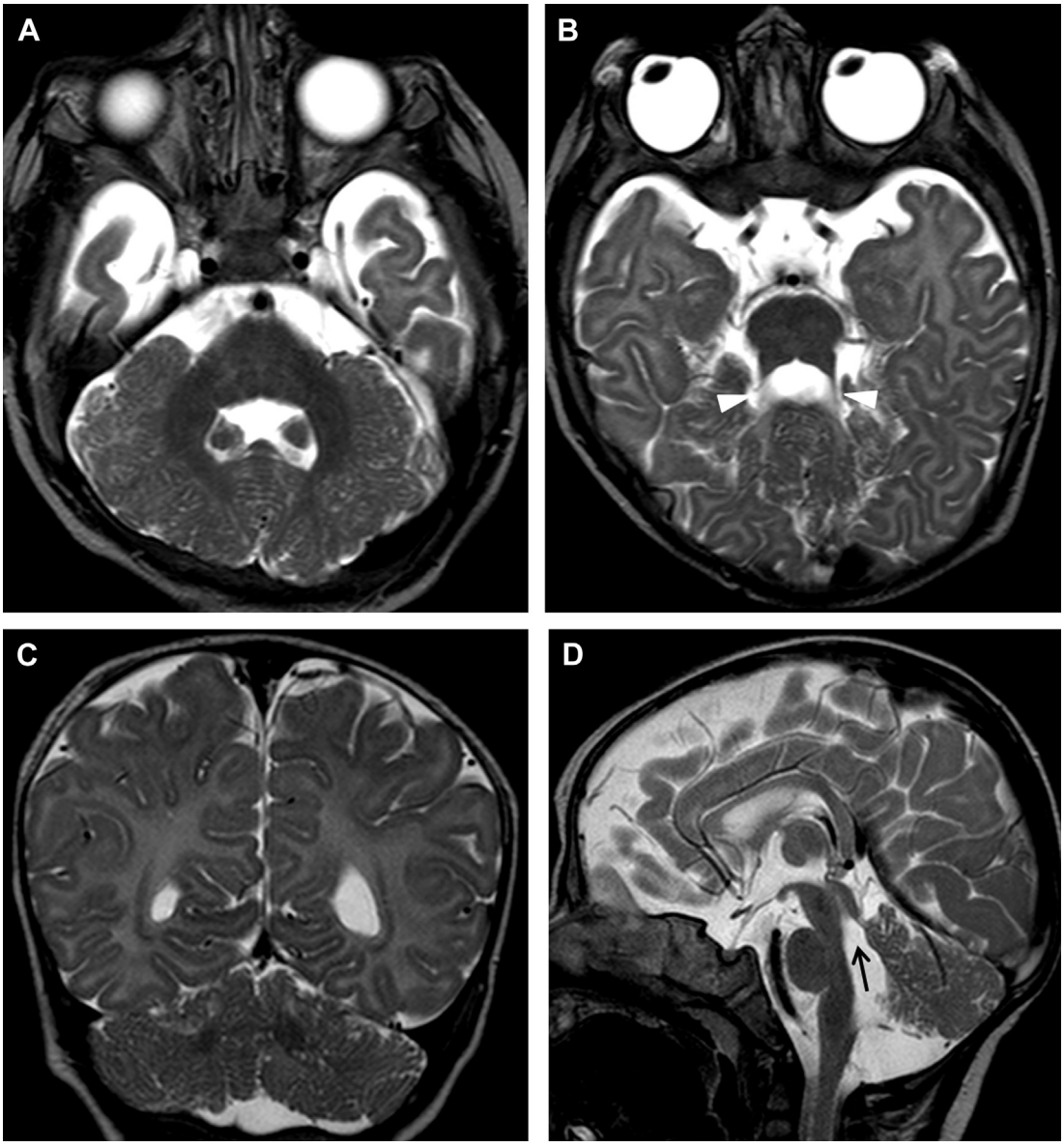

Fig. 6. Poretti-Boltshauser syndrome. (*A*, *B*) Axial and (*C*) coronal T2-weighted MR images reveal diffuse abnormal foliation with multiple cortical-subcortical cysts and thin splayed SCP (molar tooth-like sign, *arrowheads*). (*D*) Midsagittal T2-weighted image shows an enlarged, elongated, and squarelike fourth ventricle (*arrow*). The cerebral cortex is normal.

cataract.[24] The neuroimaging findings include the following (see **Fig. 9**):

- Microcephaly with simplified gyral pattern
- Severe global cerebellar hypoplasia
- Pontine hypoplasia
- Normal-sized corpus callosum[24]

RELN encodes an extracellular matrix–associated glycoprotein (reelin) that is critical for the regulation of neuronal migration during cortical and cerebellar development.[25] Affected children show severe developmental disabilities, microcephaly, seizures, and congenital lymphedema. VLDLR encodes the very-low-density lipoprotein receptor, which acts as a coreceptor for the reelin pathway. VLDLR-associated disorder is characterized by nonprogressive cerebellar ataxia, moderate to profound intellectual disability, dysarthria, strabismus, and seizures.[26] In patients with RELN-related and VLDLR-related disorders, pachygyria

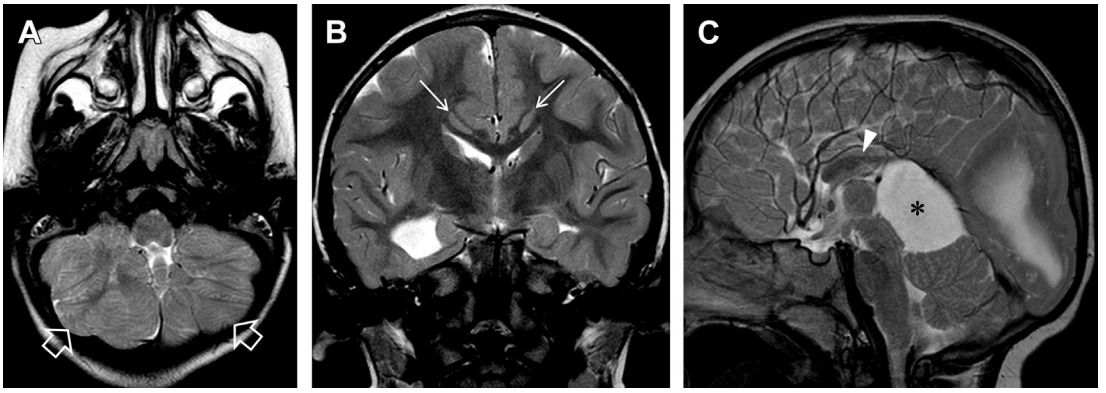

Fig. 7. Chudley-McCullough syndrome. (*A*) Axial, (*B*) coronal, and (*C*) sagittal T2-weighted MR images demonstrate abnormal foliation involving the cerebellar hemispheres (*open arrows*), bilateral cingulate subcortical gray matter heterotopia (*arrows*), partial callosal agenesis (*arrowhead*), and an arachnoid cyst in the quadrigeminal plate cistern (*asterisk*).

Table 3
Clinicoradiological features of genetic cerebellar dysplasias

Disease	Genes	Dysplasia Pattern	Associated Features
Alpha dystroglycanopathies	>15 genes	Global cerebellar dysplasia with multiple cysts	CMD, increased CK level, cobblestone malformation, supratentorial WM signal abnormalities, brainstem kinking, eye involvement
LAMB1-related cobblestone malformation	LAMB1	Global cerebellar dysplasia with multiple cysts	Variable muscular or ocular abnormalities, cobblestone malformation, supratentorial WM signal abnormalities
GPR56-related and COL3A1-related PMG and cerebellar dysplasia	GPR56, COL3A1	Global cerebellar dysplasia with multiple cysts	Bifrontal PMG, supratentorial WM signal abnormalities
Poretti-Boltshauser syndrome	LAMA1	Global cerebellar dysplasia with multiple cysts	Myopia, retinal abnormality
Chudley-McCullough syndrome	GPSM2	Abnormal foliation/ fissuration inferior hemispheres	Hearing loss, frontal and cingulate PMG/ heterotopia, partial callosal agenesis
Tubulinopathies	TUBA1A, TUBA8, TUBB2A, TUBB2B, TUBB3, TUBB5, TUBG1	Diagonal folia across vermis	Dysmorphic basal ganglia, cortical malformations, callosal dysgenesis, asymmetric brainstem
Joubert Syndrome (Ciliopathy)	>30 genes	Dysplastic superior and hypoplastic inferior vermis and hemispheres	Molar tooth sign, variably associated supratentorial malformations

Abbreviations: CK, creatine kinase; CMD, congenital muscular dystrophy; WM, white matter.

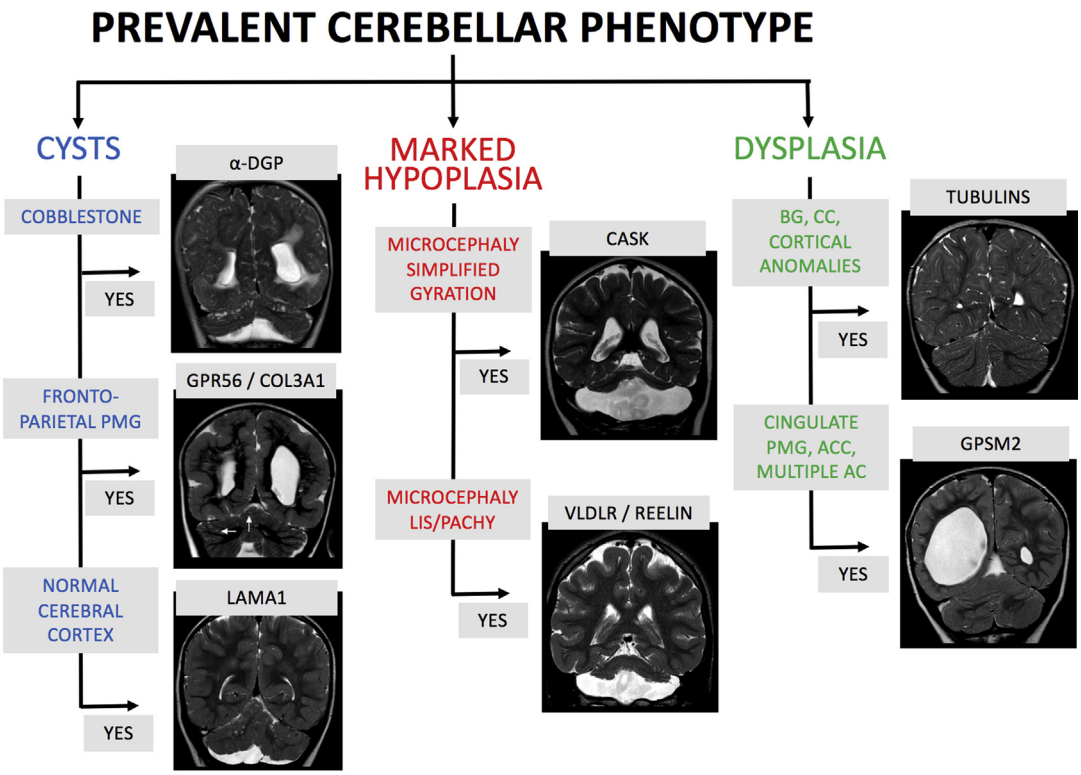

Fig. 8. Graphic flowchart for reviewing MR imaging scans displaying sigs of cerebellar dysplasia. AC, arachnoid cyst; ACC, agenesis of the corpus callosum; BG, basal ganglia; CC, corpus callosum; CASK, calcium/calmodulin-dependent serine protein kinase gene; COL3A1, collagen, type III, alpha-1 gene; GPR56, G protein-coupled receptor 56 gene; GPSM2, G Protein Signaling Modulator 2 gene; LAMA1, Laminin Subunit Alpha 1 gene; VLDLR, Very Low Density Lipoprotein Receptor gene; α-DGP, alpha-dystroglycanopathies.

(more severe in patients with RELN mutations) and extreme cerebellar hypoplasia with absent cerebellar folia and preferential vermian involvement (especially in VLDLR mutations) are characteristic neuroimaging features (see Fig. 9).[5,26]

Finally, PCH is found in congenital muscular dystrophies, resulting from mutations in genes responsible for the O-glycosylation and rarely N-glycosylation of alpha-dystroglycans.[27] Recessive mutations in these genes cause overlapping phenotypes characterized by muscular (weakness, hypotonia, and increased creatine kinase values), cerebral (intellectual disability, seizures, and tetraspasticity), and ocular (microphthalmia, optic nerve hypoplasia, chorioretinal coloboma, cataract, glaucoma, or high myopia) involvement. Based on the severity of the findings, different phenotypes have been described (in order of increasing severity): Fukuyama congenital muscular dystrophy, muscle-eye-brain disease, and Walker-Warburg syndrome.[27]

Infratentorial neuroimaging findings include the following (Fig. 10):

- Pontocerebellar hypoplasia
- Cerebellar dysplasia with subcortical cysts
- Dysplastic tectum
- Ventral pontine cleft
- Brainstem kinking

Supratentorial findings comprise the following:

- Mild ventriculomegaly to severe hydrocephalus
- White matter abnormalities/hypomyelination
- Cobblestone cortex[27]

Tubulinopathies

Tubulinopathies are a group of brain malformations caused by mutations of α- and β-tubulin genes (see Table 3).[20,28,29] Most of these mutations are de novo without risk of recurrence. Children present with variable degrees of intellectual disability, tetraspastic cerebral palsy, postnatal microcephaly, and early-onset therapy-resistant seizures. Dysmorphic features are rare, and other organs are not affected.

The spectrum of posterior fossa abnormalities includes the following (Fig. 11)[20,28,29]:

- Different degrees of PCH
- Cerebellar dysplasia with typical diagonal hemispheric cleft involving the superior vermis

Table 4
Pontocerebellar hypoplasia subtypes

Subtype	Clinical Features	Neuroimaging Features Associated with PCH	Subcategory and Gene
PCH1	Motor neuron degeneration, muscle weakness, hypotonia, respiratory insufficiency, congenital contractures, early death	Variable pontine involvement, CC hypoplasia, cortical atrophy, incomplete myelination	PCH1A: VRK1 PCH1B: EXOSC3 PCH1C: EXOSC8 PCH1D: SLC25A46
PCH2	Generalized clonus, impaired swallowing, dystonia, chorea, progressive microcephaly	Involvement hemispheres >> vermis (dragonfly appearance), hemispheric cavitations, cerebral atrophy	PCH2A: TSEN54 PCH2B: TSEN2 PCH2C: TSEN34 PCH2D: SEPSECS PCH2E: VPS53 PCH2F: TSEN15
PCH3	Facial dysmorphisms, optic nerve atrophy, progressive microcephaly	Optic nerve atrophy, thin corpus callosum	PCLO
PCH4	Severe form of PCH2 with congenital contractures, microcephaly, polyhydramnios	Severe cerebral atrophy, subdural fluid collections	TSEN54
PCH5	Same as PCH4	Severe cerebral atrophy, subdural fluid collections, involvement vermis >> hemispheres	TSEN54
PCH6	Hypotonia, seizures, elevated CSF lactate	Rapidly progressive supratentorial and infratentorial atrophy	RARS2
PCH7	Disorder of sexual development	Severe WM reduction, enlarged ventricles	TOE1
PCH8	Abnormal muscle tone, dystonia, ataxia, no/little progression	Proportionate involvement of vermis and hemispheres, nonprogressive course	CHMP1A
PCH9	Abnormal muscle tone, impaired swallowing, progressive microcephaly	Callosal dysgenesis, "figure-of-8" midbrain appearance, small hyperintense basal ganglia, and hypointense thalami	AMPD2
PCH10	Abnormal muscle tone, seizures, motor neuron degeneration, microcephaly	Mild cerebellar hypoplasia/atrophy, thin corpus callosum, myelination delay	CLP1
PCH11	severe neurodevelopmental delay, microcephaly, hypotonia	Nonprogressive PCH, callosal hypoplasia	TBC1D23

- Asymmetric midbrain and pons with clefts
- Asymmetric cerebral peduncles

Characteristic supratentorial findings are as follows[20,28,29]:

- Cortical malformations (lissencephaly, polymicrogyria, and dysgyria)
- Dysmorphic basal ganglia due to internal capsule anomalies
- Dysmorphic ventriculomegaly
- Agenesis/dysgenesis of the corpus callosum and anterior commissure

DTI and FT studies may reveal axonal pathfinding anomalies, including anterior commissure absence, abnormal callosal connectivity, reduced transverse pontine fibers with slanting course, and small asymmetric corticospinal tracts.[20,28,29]

Joubert syndrome

Joubert syndrome refers to a group of rare conditions, also called ciliopathies, that stem from defects in a cellular organelle, the primary nonmotile cilium. Primary cilia play a key role in the development and functioning of various cells, including

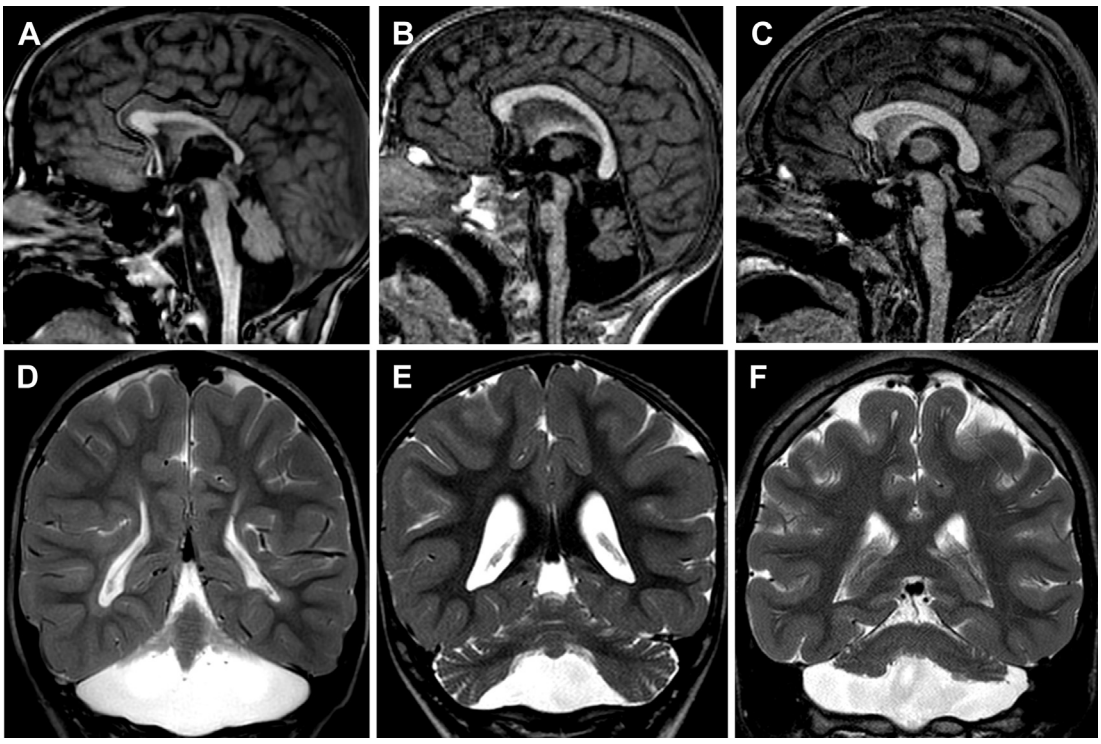

Fig. 9. PCHs. PCH 2: (*A*) midsagittal T1-weighted and (*D*) coronal T2-weighted MR images reveal marked hypoplasia of the pons and cerebellum with more severe involvement of the cerebellar hemispheres relative to the vermis ("dragonfly" appearance). Callosal hypoplasia is also noted. CASK-related PCH: (*B*) midsagittal T1-weighted and (*E*) coronal T2-weighted MR images demonstrate hypoplasia of the pons and cerebellum with proportionate involvement of the cerebellar hemispheres relative to the vermis. The signal intensity of the cerebellar hemispheres is normal (in contrast with PCH 2). Microcephaly with simplified gyral pattern is also noted. VLDLR-related PCH: (*C*) midsagittal T1-weighted and (*F*) coronal T2-weighted MR images show hypoplasia of the pons and cerebellum with typical absence of cerebellar foliation and preferential vermian involvement. Note the associated lissencephaly.

retinal photoreceptors, epithelial cells lining the renal tubules, bile ducts, and neurons.[30,31] In the CNS, they are implicated in neuronal cell proliferation and axonal migration in the cerebellum and brainstem. Ciliopathies are characterized by an extreme genetic heterogeneity, with more than 30 genes identified so far. Mutations in all these genes but OFD1 are autosomal recessively inherited, resulting in a recurrence risk of 25%.[30,31] Affected patients typically present with ocular (colobomas, retinal dystrophy), hepatic (congenital hepatic fibrosis), skeletal (different forms of polydactyly), and renal (nephronophthisis) abnormalities. Common neurologic symptoms include hypotonia, breathing abnormalities, variable intellectual disability, ataxia, and ocular motor apraxia.[30] The "molar tooth sign" observed on axial neuroimaging is required for the diagnosis and is defined by elongated, thickened, and horizontally orientated SCP, a deep interpeduncular fossa, and vermian hypoplasia (**Fig. 12**).[30–32] Of note, the degree of vermian hypoplasia, shape of the "molar tooth," size of the posterior fossa, and degree of cerebellar hypodysplasia are variable. Brainstem abnormalities are present in about 30% of cases, including a dysmorphic tectum and midbrain, thickened and elongated midbrain, and small pons.[32] Supratentorial anomalies are detected in about 30% of cases:

- Callosal dysgenesis
- Encephaloceles
- Hypothalamic hamartomas (in oral facial digital syndrome type VI)
- Cortical malformations
- Ventriculomegaly

Differences in neuroimaging findings can be present within siblings representing an intrafamilial heterogeneity.[32] Except for oral facial digital syndrome type VI, no neuroimaging-genotype correlations are known. DTI reveals underlying defects of axonal guidance, including lack of

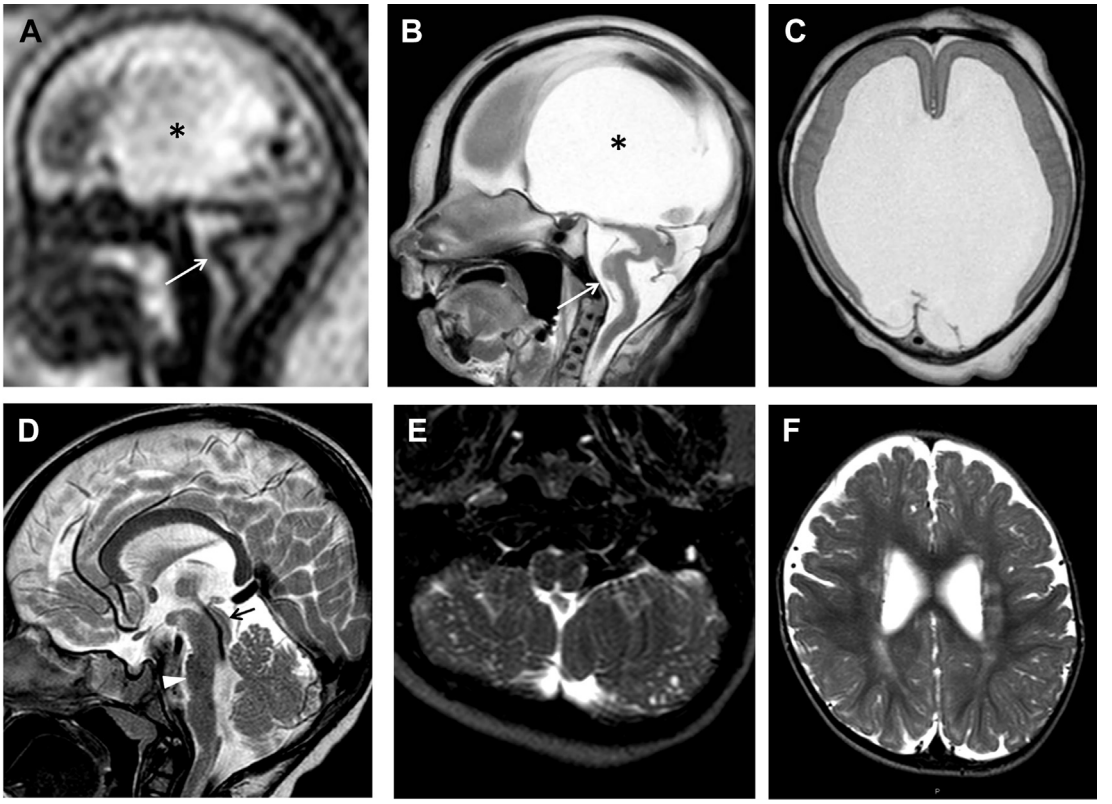

Fig. 10. Alpha-dystroglycanopathies. (*A*) Fetal MR imaging, midsagittal T2-weighted image, and (*B*, *C*) matching postmortem midsagittal and axial T2-weighted MR images, performed in a fetus with Walker-Warburg syndrome (21 gestational weeks), demonstrate severe supratentorial hydrocephalus (*asterisks*) with marked kinking of the brainstem (*arrows*). (*D*) Sagittal and (*E*) axial T2-weighted MR images in a child with muscle-eye-brain disease show a dysplastic midbrain and tectum (*arrow*), a thinned pons (*arrowhead*), multiple bilateral subcortical cysts in the cerebellar hemispheres, mild ventriculomegaly, multifocal white matter changes, and cobblestone malformation (*F*).

SCP decussation,[6] abnormal corticospinal tracts course (decaying molar tooth),[33] and ectopic transverse white matter tracts in the ventral midbrain (anterior mesencephalic cap dysplasia).[34]

Predominant Brainstem Malformations

Pontine tegmental cap dysplasia

Pontine tegmental cap dysplasia is a rare sporadic brainstem malformation with unknown genotype and no familial recurrence.[35] Clinically, it is characterized by cranial nerve deficits (including hearing loss, facial paralysis, trigeminal anesthesia, and dysphagia), cognitive disability, and ataxia. The degree of brainstem dysplasia grossly correlates with the developmental disability. Vertebral segmentation anomalies, rib malformations, and congenital heart defects have also been observed.

Neuroimaging findings include the following[7,35,36] (**Fig. 13**):

- Ventral pons flattening
- A vaulted pontine tegmentum (the cap)
- Small asymmetric middle cerebellar peduncles
- Inferior cerebellar peduncles agenesis
- Vermian hypoplasia
- Molar toothlike aspect of the ponto-mesencephalic junction
- Absent inferior olivary prominence
- Duplicated internal auditory canals
- Hypoplastic cranial nerves

DTI shows absence of the transverse pontine fibers and SCP decussation, and presence of a transverse axonal band at the level of the "cap" along the dorsal pons.[4,7]

Horizontal gaze palsy with progressive scoliosis

Horizontal gaze palsy with progressive scoliosis is a rare autosomal recessive disorder caused by

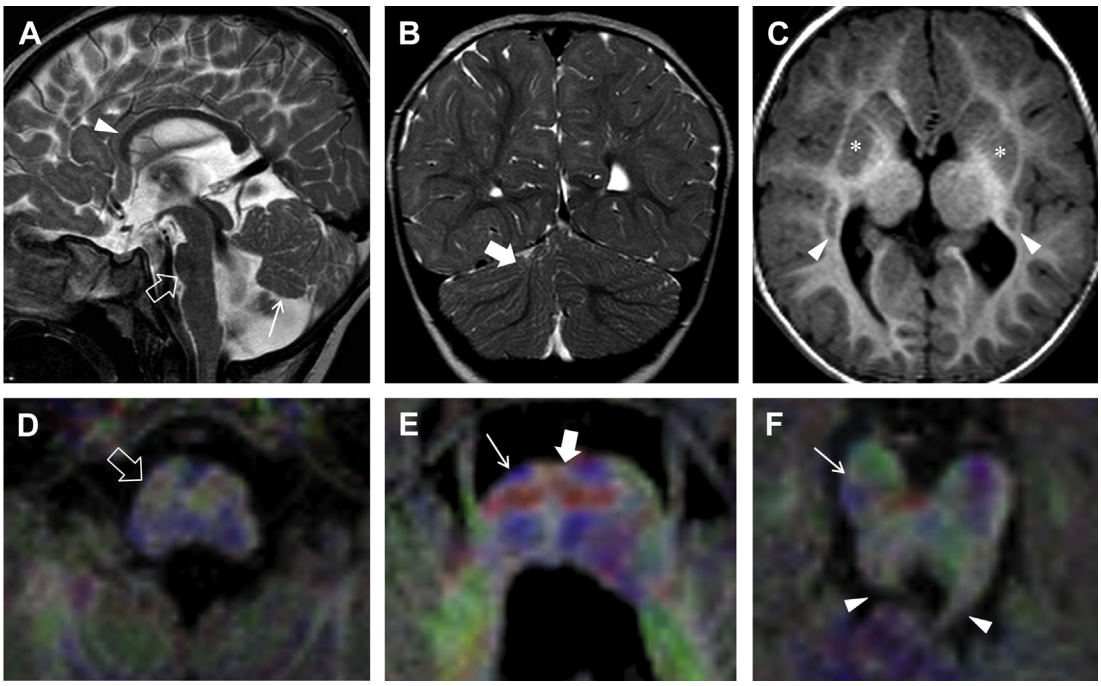

Fig. 11. Tubulinopathy. (*A*) Sagittal and (*B*) coronal T2-weighted MR images reveal callosal hypo-dysgenesis (*arrowhead*), pontine hypoplasia (*open arrow*), a smaller and slightly upward rotated vermis (*arrow*), and right unilateral cerebellar dysplasia with oblique folia (*thick arrow*). (*C*) Axial 3D T1-weighted MR image demonstrates dysmorphic basal ganglia (*asterisks*), diffuse dysgyria, and subcortical gray matter heterotopias (*arrowheads*). (*D–F*) Axial color-coded FA maps overlaid to axial 3D T1-weighted images, magnified views, show enlargement of the right portion of medulla (*open arrow*), pontine, and midbrain asymmetry with smaller right corticospinal tract (*arrows*), reduced anterior transverse pontine fibers (*thick arrow*), and dysmorphic SCP (*arrowheads*).

mutations in ROBO3, encoding a receptor required for axonal guidance.[37–39] Affected children have congenital absence of horizontal eye movements, preservation of vertical gaze and convergence, and progressive scoliosis. Neurocognitive functions are typically preserved.[37–39]

Neuroimaging findings include the following (**Fig. 14**):

- A butterfly-shaped medulla, due to the missing prominence of the gracile and cuneate nuclei

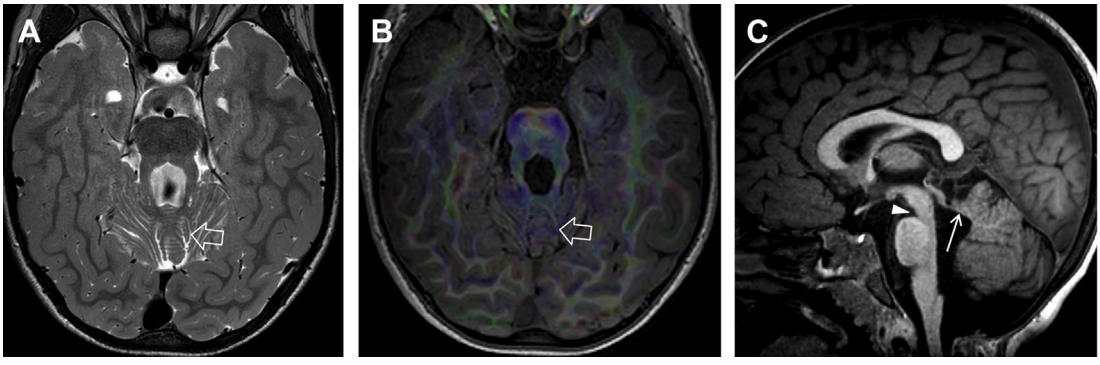

Fig. 12. Joubert syndrome. (*A*) Axial T2-weighted and (*B*) FA color-coded FA map overlaid to 3D T1-weighted MR images show the molar tooth sign characterized by elongated, thickened, and horizontally oriented SCP and a deep interpeduncular fossa. (*C*) Sagittal T1-weighted MR image reveals hypoplasia and dysplasia of the vermis (*open arrow*), enlargement of the fourth ventricle with upward and posterior displacement of the fastigium (*arrow*), and a narrow pontomesencephalic isthmus (*arrowhead*).

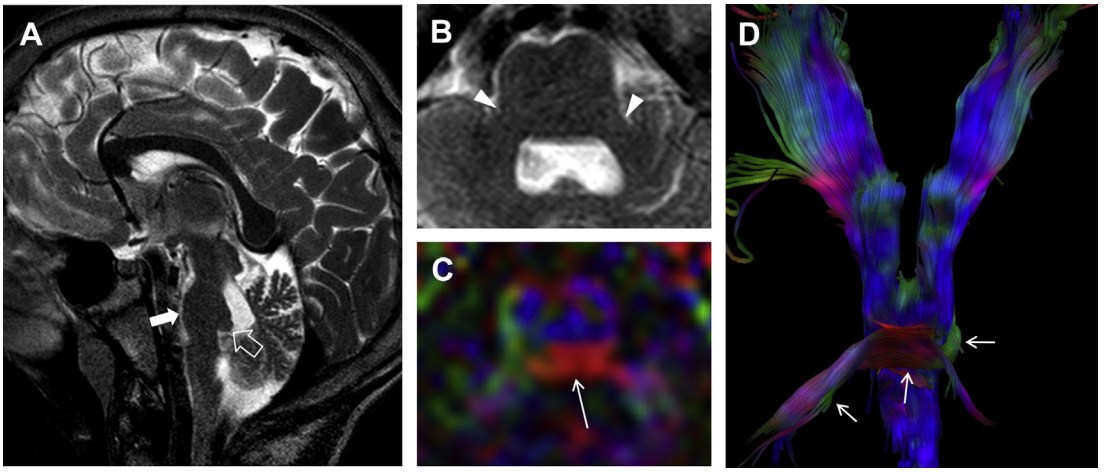

Fig. 13. Pontine tegmental cap dysplasia. (*A*) Midsagittal T2-weighted image demonstrates a flattened ventral pons (*arrow*), a cap covering the dorsal pons and protruding into the fourth ventricle (*open arrow*). (*B*) Axial T2-weighted and (*C*) and FA color-coded FA map overlaid to 3D T1-weighted MR images show bilateral hypoplastic MCP (*arrowheads*), absence of the normal pontocerebellar transverse fibers, and an aberrant dorsal transverse axonal band at the level of the cap along the dorsal pons (*arrow*). (*D*) FT reconstruction, posterior view, reveals the misoriented fibers connecting the basal pons to the cerebellar hemisphere through the MCP (*arrows*).

- Pontine hypoplasia with dorsal midline cleft
- Absence of the facial colliculi bulging contour
- Prominence of inferior olivary nuclei

DTI typically shows absence of the decussation of corticospinal tracts, pontine sensory tracts, and SCP.[5,39]

Diencephalic-mesencephalic junction dysplasia

Diencephalic-mesencephalic junction dysplasia is characterized by dorsoventral enlargement and abnormal butterfly-like contour of the midbrain on axial sections.[40] Clinical features include cognitive impairment, axial hypotonia, spastic tetraparesis, and seizures. Recently, mutations in the protocadherin-12 gene, encoding a cell surface protein promoting cell adhesion and neurite outgrowth, have been identified in some of these patients.[41] Additional features include ventriculomegaly, PCH, calcifications, and abnormalities of the corticospinal tracts, commissures, basal ganglia, and olfactory bulbs.[42,43] Recently, the

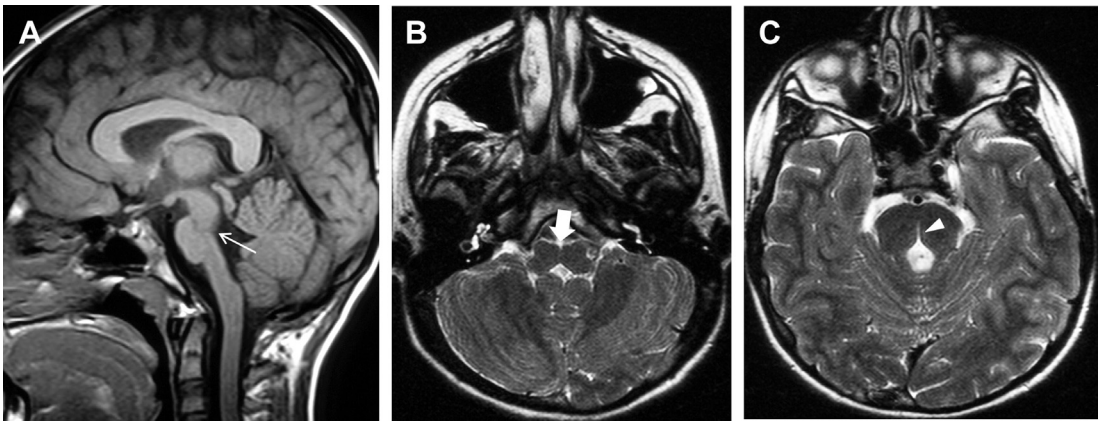

Fig. 14. Horizontal gaze palsy with progressive scoliosis. (*A*) Midsagittal T1-weighted and (*B*, *C*) axial T2-weighted MR images show depression of the floor of the fourth ventricle (*arrow*), a butterfly medulla with more prominent inferior olivary nuclei compared with the pyramids (*thick arrow*), and a deep dorsal midline pontine cleft (*arrowhead*).

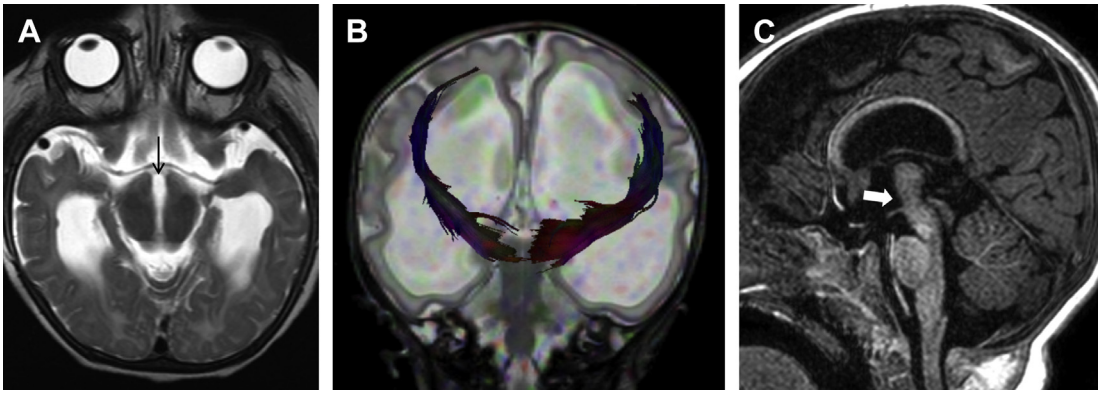

Fig. 15. Diencephalic-mesencephalic junction dysplasia (DMJD). (*A*) Axial T2-weighted MR image of a child with type A DMJD shows fusion of the hypothalamus and midbrain, enlargement of the dorsoventral axis of the midbrain, and ventral midbrain cleft (*arrow*) resulting in a butterfly-like appearance. (*B*) FT superimposed to a coronal T2-weighted MR image reveals abrupt interruption of the corticospinal tracts at the level of the midbrain in another patient with type A DMJD. (*C*) Sagittal 3D T1-weighted MR image demonstrates fusion of the midbrain with the interthalamic mass (*arrow*) in a patient with type B DMJD.

spectrum of diencephalic-mesencephalic junction anomalies has expanded, including the following (**Fig. 15**):

- Type A forms with complete hypothalamic-mesencephalic fusion leading to dorsoventral enlargement and abnormal contour of the midbrain on axial planes, variably associated with a ventral cleft or linear T2-hyperintensities.
- Type B forms are characterized by incomplete cleavage between the thalami and the mesencephalon on the sagittal plane, variably associated with brainstem and/or vermian hypoplasia.

DTI shows an abrupt arrest of corticospinal tracts at the level of the diencephalon, suggesting disturbed axonal path-finding.[40,42]

SUMMARY

Posterior fossa malformations represent a wide variety of disorders that may involve different parts of the pons and cerebellum. Neuroimaging plays a key role in the diagnosis of these conditions with well-defined neuroimaging-based diagnostic criteria. Accurate classification of cerebellar and brainstem malformations is important for therapy, prognosis, and genetic counseling. In addition, advanced neuroimaging, including DTI and FT, may provide important information about the pathogenesis, serving as a biomarker for cognitive outcome in selected cerebellar and brainstem malformations.

ACKNOWLEDGMENTS

This work was supported by funds from Current Research for the 2018-2020 triennium – Research Line 5 on Muscular and Neurological Disorders – Ministry of Health—Italy.

REFERENCES

1. Barkovich AJ, Millen KJ, Dobyns WB. A developmental and genetic classification for midbrain-hindbrain malformations. Brain 2009; 132(Pt 12):3199–230.
2. Doherty D, Millen KJ, Barkovich AJ. Midbrain and hindbrain malformations: advances in clinical diagnosis, imaging, and genetics. Lancet Neurol 2013; 12(4):381–93.
3. Poretti A, Boltshauser E, Huisman TA. Cerebellar and brainstem malformations. Neuroimaging Clin N Am 2016;26(3):341–57.
4. Jissendi-Tchofo P, Severino M, Nguema-Edzang B, et al. Update on neuroimaging phenotypes of mid-hindbrain malformations. Neuroradiology 2015; 57(2):113–38.
5. Poretti A, Meoded A, Rossi A, et al. Diffusion tensor imaging and fiber tractography in brain malformations. Pediatr Radiol 2013;43(1):28–54.
6. Poretti A, Boltshauser E, Loenneker T, et al. Diffusion tensor imaging in Joubert syndrome. AJNR Am J Neuroradiol 2007;28(10):1929–33.
7. Jissendi-Tchofo P, Doherty D, McGillivray G, et al. Pontine tegmental cap dysplasia: MR imaging and diffusion tensor imaging features of impaired axonal navigation. AJNR Am J Neuroradiol 2009;30(1):113–9.
8. Garel C. Posterior fossa malformations: main features and limits in prenatal diagnosis. Pediatr Radiol 2010;40(6):1038–45.
9. Aldinger KA, Lehmann OJ, Hudgins L, et al. FOXC1 is required for normal cerebellar development and is a

major contributor to chromosome 6p25.3 Dandy-Walker malformation. Nat Genet 2009;41(9):1037–42.
10. Alexiou GA, Sfakianos G, Prodromou N. Dandy-Walker malformation: analysis of 19 cases. J Child Neurol 2010;25(2):188–91.
11. Correa GG, Amaral LF, Vedolin LM. Neuroimaging of Dandy-Walker malformation: new concepts. Top Magn Reson Imaging 2011;22(6):303–12.
12. Ishak GE, Dempsey JC, Shaw DW, et al. Rhombencephalosynapsis: a hindbrain malformation associated with incomplete separation of midbrain and forebrain, hydrocephalus and a broad spectrum of severity. Brain 2012;135(Pt 5):1370–86.
13. Sukhudyan B, Jaladyan V, Melikyan G, et al. Gomez-Lopez-Hernandez syndrome: reappraisal of the diagnostic criteria. Eur J Pediatr 2010;169(12):1523–8.
14. Whitehead MT, Choudhri AF, Grimm J, et al. Rhombencephalosynapsis as a cause of aqueductal stenosis: an under-recognized association in hydrocephalic children. Pediatr Radiol 2014;44(7):849–56.
15. Boltshauser E, Scheer I, Huisman TA, et al. Cerebellar cysts in children: a pattern recognition approach. Cerebellum 2015;14(3):308–16.
16. Doherty D, Chudley AE, Coghlan G, et al. GPSM2 mutations cause the brain malformations and hearing loss in Chudley-McCullough syndrome. Am J Hum Genet 2012;90(6):1088–93.
17. Bahi-Buisson N, Poirier K, Boddaert N, et al. GPR56-related bilateral frontoparietal polymicrogyria: further evidence for an overlap with the cobblestone complex. Brain 2010;133(11):3194–209.
18. Vandervore L, Stouffs K, Tanyalçin I, et al. Bi-allelic variants in COL3A1 encoding the ligand to GPR56 are associated with cobblestone-like cortical malformation, white matter changes and cerebellar cysts. J Med Genet 2017;54(6):432–40.
19. Micalizzi A, Poretti A, Romani M, et al. Clinical, neuroradiological and molecular characterization of cerebellar dysplasia with cysts (Poretti-Boltshauser syndrome). Eur J Hum Genet 2016;24(9):1262–7.
20. Romaniello R, Arrigoni F, Panzeri E, et al. Tubulin-related cerebellar dysplasia: definition of a distinct pattern of cerebellar malformation. Eur Radiol 2017;27(12):5080–92.
21. Poretti A, Boltshauser E, Huisman TA. Prenatal cerebellar disruptions: neuroimaging spectrum of findings in correlation with likely mechanisms and etiologies of injury. Neuroimaging Clin N Am 2016;26(3):359–72.
22. van Dijk T, Baas F, Barth PG, et al. What's new in pontocerebellar hypoplasia? An update on genes and subtypes. Orphanet J Rare Dis 2018;13(1):92.
23. Accogli A, Iacomino M, Pinto F, et al. Novel AMPD2 mutation in pontocerebellar hypoplasia, dysmorphisms, and teeth abnormalities. Neurol Genet 2017;3(5):e179.
24. Burglen L, Chantot-Bastaraud S, Garel C, et al. Spectrum of pontocerebellar hypoplasia in 13 girls and boys with CASK mutations: confirmation of a recognizable phenotype and first description of a male mosaic patient. Orphanet J Rare Dis 2012;7:18.
25. Hong SE, Shugart YY, Huang DT, et al. Autosomal recessive lissencephaly with cerebellar hypoplasia is associated with human RELN mutations. Nat Genet 2000;26(1):93–6.
26. Valence S, Garel C, Barth M, et al. RELN and VLDLR mutations underlie two distinguishable clinico-radiological phenotypes. Clin Genet 2016;90(6):545–9.
27. Clement E, Mercuri E, Godfrey C, et al. Brain involvement in muscular dystrophies with defective dystroglycan glycosylation. Ann Neurol 2008;64(5):573–82.
28. Romaniello R, Arrigoni F, Cavallini A, et al. Brain malformations and mutations in alpha- and beta-tubulin genes: a review of the literature and description of two new cases. Dev Med Child Neurol 2014;56(4):354–60.
29. Arrigoni F, Romaniello R, Peruzzo D, et al. The spectrum of brainstem malformations associated to mutations of the tubulin genes family: MRI and DTI analysis. Eur Radiol 2019;29(2):770–82.
30. Romani M, Micalizzi A, Valente EM. Joubert syndrome: congenital cerebellar ataxia with the molar tooth. Lancet Neurol 2013;12(9):894–905.
31. Hildebrandt F, Benzing T, Katsanis N. Ciliopathies. N Engl J Med 2011;364(16):1533–43.
32. Poretti A, Snow J, Summers AC, et al. Joubert syndrome: neuroimaging findings in 110 patients in correlation with cognitive function and genetic cause. J Med Genet 2017;54(8):521–9.
33. Alves CAPF, Ferraciolli S, Matsui C, et al. Decaying molar tooth sign in Joubert syndrome and related disorders is correlated to a displacement of the corticospinal tract. Neuroradiology 2017;59(12):1189–91.
34. Arrigoni F, Romaniello R, Peruzzo D, et al. Anterior mesencephalic cap dysplasia: novel brain stem malformative features associated with Joubert syndrome. AJNR Am J Neuroradiol 2017;38(12):2385–90.
35. Barth PG, Majoie CB, Caan MW, et al. Pontine tegmental cap dysplasia: a novel brain malformation with a defect in axonal guidance. Brain 2007;130(Pt 9):2258–66.
36. Desai NK, Young L, Miranda MA, et al. Pontine tegmental cap dysplasia: the neurotologic perspective. Otolaryngol Head Neck Surg 2011;145(6):992–8.

37. Bosley TM, Salih MA, Jen JC, et al. Neurologic features of horizontal gaze palsy and progressive scoliosis with mutations in ROBO3. Neurology 2005; 64(7):1196–203.
38. Rossi A, Catala M, Biancheri R, et al. MR imaging of brain-stem hypoplasia in horizontal gaze palsy with progressive scoliosis. AJNR Am J Neuroradiol 2004;25(6):1046–8.
39. Haller S, Wetzel SG, Lutschg J. Functional MRI, DTI and neurophysiology in horizontal gaze palsy with progressive scoliosis. Neuroradiology 2008;50(5): 453–9.
40. Zaki MS, Saleem SN, Dobyns WB, et al. Diencephalic-mesencephalic junction dysplasia: a novel recessive brain malformation. Brain 2012;135(Pt 8): 2416–27.
41. Guemez-Gamboa A, Çağlayan AO, Stanley V, et al. Loss of protocadherin-12 leads to diencephalic-mesencephalic junction dysplasia syndrome. Ann Neurol 2018;84(5):638–47.
42. Severino M, Tortora D, Pistorio A, et al. Expanding the spectrum of congenital anomalies of the diencephalic-mesencephalic junction. Neuroradiology 2016;58(1):33–44.
43. Severino M, Righini A, Tortora D, et al. MR imaging diagnosis of diencephalic-mesencephalic junction dysplasia in fetuses with developmental ventriculomegaly. AJNR Am J Neuroradiol 2017;38(8):1643–6.